CHEMISTRY OF MATERIALS

pubs.acs.org/cm

Article

Single-Precursor Intermediate Shelling Enables Bright, Narrow Line Width InAs/InZnP-Based QD Emitters

Laxmi Kishore Sagar, Golam Bappi, Andrew Johnston, Bin Chen, Petar Todorović, Larissa Levina, Makhsud I. Saidaminov, F. Pelayo García de Arquer, Sjoerd Hoogland, and Edward H. Sargent*

Cite This: https://dx.doi.org/10.1021/acs.chemmater.9b05110

Read Online

ACCESS | Metrics & More | Article Recommendations | Supporting Information

ABSTRACT: Bright, narrow spectrum infrared emitters, particularly Cd- and Pb-free materials, are of interest for bioimaging, photodetection, and telecommunications. InAs-based quantum dots (QDs) are promising emitters in this spectral range; however, efforts to increase the photoluminescence quantum yield (PLQY) tend to broaden the PL line width as a consequence of interfacial defect formation when thick shells, lattice-mismatched with the core, are employed. Here we report that developing a single-precursor complex for InZnP growth enables uniform shell growth that maintains the excellent size dispersion (6%) of the cores. The introduction of this intermediate layer is key to facilitate the subsequent growth of different shells to improve radiative recombination without sacrificing size uniformity. The growth of InAs/InZnP/ZnSe leads to a PL full-width at half-maximum (fwhm) of 100 meV at 1.12 eV with a PLQY of 14%. We then further introduce an additional GaP layer to increase the radiative/nonradiative relative rate. InAs/InZnP/GaP/ZnSe QDs reach a PLQY of 23% while maintaining a narrow fwhm.

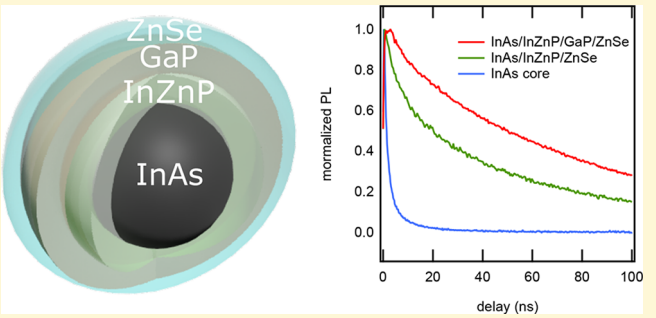

INTRODUCTION

Colloidal quantum dots (CQDs) exhibit size-dependent optoelectronic properties due to quantum confinement.[1,2] CQDs find use in displays,[3] LEDs,[4,5] lasers,[6,7] photodetection,[8] night vision,[9] telecommunications,[10] solar cells,[11] and bioimaging.[12]

There has been a concerted effort to develop Pb- and Cd-free QDs as inorganic fluorophores. III−V binary semiconductors such as InP, InAs, and InSb have attracted interest as a result.[13,14]

Unfortunately, as-synthesized III−V QDs suffer from low photoluminescence quantum yields (PLQY) of 1−2%: the surfaces of III−V QDs are prone to oxidation due to the high oxygen affinity of the anion, and this increases nonradiative recombination.[15] The growth of an epitaxial, wide-bandgap shell around the quantum dot passivates and protects the QD surface while confining the charge carriers to the core and increasing radiative efficiency.[16]

Desired in shell growth are a minimal lattice strain at the core/shell interface and a suitable energetic band offset that spatially confines the electron−hole pair to the core. Synthetic efforts on InP QD shelling have led to InP/ZnS, InP/GaP/ZnS, and InP/ZnSe/ZnS QDs that exhibit near-unity PLQY.[17−19] As a result, InP shelled dots are increasingly replacing CdSe QDs as color converters in commercial QD displays.

InAs (with a bandgap of 0.35 eV) is an attractive choice as a fluorophore for near-infrared (NIR) emission.[13] Wide-bandgap II−VI semiconductors such as CdSe, CdS, ZnSe, and ZnS are used as shells (see Supporting Information, Table S1, for lattice mismatch).[20,21] In the search for Cd- and Pb-free shell materials, ZnSe and ZnS share the zincblende crystal structure with InAs QDs and are thus in principle well-suited for shelling. However, the lattice mismatch of ZnSe and ZnS (6.4 and 10.7%, respectively) limits the shell thickness to a few monolayers.[20] Another problem associated with established shelling approaches is the increase in size dispersion after shell growth, leading to broader PL line widths. There is a need to develop an approach that allows the growth of thick shells to increase confinement and passivation while maintaining sharp PL line widths.

Here we report InAs/InZnP/GaP/ZnSe QDs and find that these provide sharp absorption spectral features and narrow emission (line widths ≈ 100 meV). In particular, we show that the core/shell QDs synthesized using this approach retain the narrow PL line widths of the starting InAs cores. We also find

Received: December 10, 2019
Revised: March 9, 2020
Published: March 10, 2020

that the addition of a GaP layer improves the PLQY by ∼1.7× relative to InAs/InP/ZnSe. PL decay and transient absorption (TA) show that surface passivation is improved following shell growth. These results provide insight into the development of InAs-based QDs for optoelectronic applications and are the narrowest Pb- and Cd-free IR QDs reported.

EXPERIMENTAL SECTION

Chemicals. Indium(III) acetate ($In(OAc)_3$, 99.99%), oleic acid (OA, tech. 90%), 1-octadecene (ODE, tech. 90%), tris(trimethylsilyl)-phosphine ($(TMSi)_3As$, 95%), zinc acetate ($Zn(OAc)_3$, 99.99%), trioctylphosphine (TOP, 97%), selenium powder (Se, 99.999%), gallium(III) chloride ($GaCl_3$, 99.99%), tetrachloroethylene (C_2Cl_4, 99%), hexane (reagent grade, >99%), oleylamine (≥98%), 1-butanol (anhydrous, 99.8%), and isopropyl alcohol (IPA, anhydrous, 99.8%) were purchased from Sigma-Aldrich and used without further purification unless stated otherwise. Zinc stearate (ZnO, 12.5−14%) was purchased from Alfa Aesar. Anhydrous ethanol and *n*-octane were purchased from Caledon. Tris(trimethylgermyl)arsine ($(TMGe)_3As$) was purchased from nanomeps. ODE was degassed under vacuum overnight in a Schlenk flask at 110 °C. Oleylamine was degassed under vacuum for 3 h at 110 °C. Then, flasks were transferred to the glovebox for use at a later step.

InAs QD Synthesis. InAs QDs were synthesized using a modified approach[22] via the continuous injection of amorphous InAs clusters into the InAs seeds. Degassed ODE was used as the solvent throughout the synthesis.

Synthesis of InAs Clusters. $In(OAc)_3$ (2.9 g, 10 mmol), oleic acid (8.50 g, 30 mmol), and ODE (50 mL) were added to a 250 mL Schlenk flask. The reaction mixture was degassed under vacuum at 110 °C for 90 min. The flow was switched to nitrogen, and the flask was cooled to room temperature. Inside a nitrogen-filled glovebox, 2.14 g (5 mmol) of $(TMGe)_3As$ was added to 5 mL of degassed ODE. The $(TMGe)_3As$ solution was injected into the $In(OAc)_3$ solution at room temperature and then stirred for an additional 30 min. The flask was transferred to the glovebox for use at a later step.

Synthesis of InAs Seeds. $In(OAc)_3$ (0.29 g, 1 mmol), oleic acid (0.85 g, 3 mmol), and ODE (5 mL) were added to a 50 mL round bottomed flask and degassed under vacuum at 110 °C for 90 min. Inside the glovebox, 0.214 g (0.5 mmol) of $(TMGe)_3As$ was dissolved in 1 mL of degassed ODE. $(TMGe)_3As$ solution was quickly injected into $In(OAc)_3$ solution at 300 °C. The growth of seeds was continued for 30 min at 270 °C.

Synthesis of InAs QDs by Continuous Injection of Amorphous Clusters. InAs cluster solution (4 mL) was taken into a syringe connected to a syringe pump. InAs clusters were added at a rate of 2 mL/hour at a growth temperature of 300 °C to the InAs seeds. To obtain the desired size of InAs QDs, we monitored the reaction by removing aliquots from the growth solution and measuring the absorption spectra. Once the desired size was obtained, we cooled the reaction mixture to room temperature, and the flask was transferred to glovebox. QDs were precipitated by the addition of 1-butanol and centrifuged at 4000 rpm for 5 min. The purification process was repeated another time after redispersion of the dots in *n*-octane. Finally, the dots were dispersed in *n*-octane at a concentration of ∼50 mg/mL. To carry out the shell growth, InAs QDs stored in the glovebox were used.

InAs/InZnP/ZnSe QD Synthesis. Shell growth was carried out utilizing a seeded growth approach in two steps (see Figure 1). First, an InZnP shell was grown on InAs QDs using a single injection of InZnP complex precursor. In a typical reaction, 1 mL of purified InAs QDs (50 mg/mL) in *n*-octane was added to a mixture of 4 mL of degassed ODE and 4 mL of degassed oleylamine in a three-neck Schlenk flask. The solution was placed under vacuum at 110 °C for 60 min to remove the *n*-octane. Subsequently, the flow was switched to nitrogen, and the solution was heated to 265 °C for the shell growth. Once the temperature reached 250 °C, the InZnP (4 mL) complex shell precursor was injected using a syringe pump at a rate of 4 mL/hour. We monitored the shell growth by taking aliquots throughout

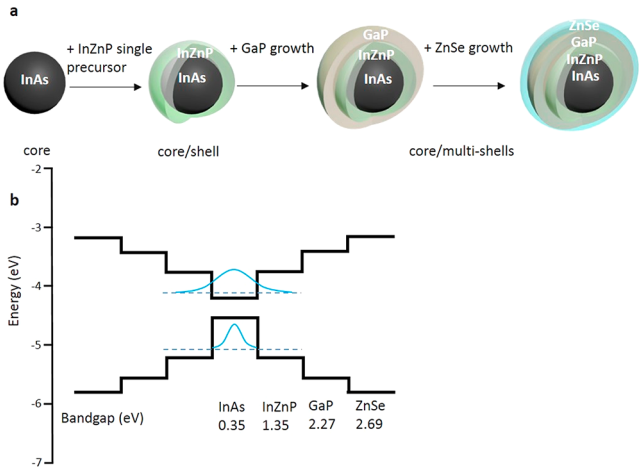

Figure 1. (a) Schematic depicting the synthesis of InAs/InZnP/GaP/ZnSe core/multishell QDs. (b) Band alignment.[18]

the growth process and measuring the absorption and PL spectra. We purified the aliquots using IPA and *n*-octane as the antisolvent and solvent, respectively. Once the growth of InZnP was completed, ZnSe shell growth was carried out at 265 °C by dropwise addition of injecting 0.5 mL of TOP-Se and 1 mL of Zn-stearate (250 mg of Zn-stearate in 1 mL of ODE) over 45 min. After the growth of ZnSe, the flask was cooled down to room temperature. The dots were purified two times using IPA and *n*-octane as antisolvent and solvent.

InAs/InZnP/GaP/ZnSe QD Synthesis. The synthesis was carried out in a similar manner to InAs/InZnP/GaP/ZnSe QDs; after the growth of the InZnP shell, Ga-oleate and TMS-P solution were added to the InAs/InZnP reaction mixture at 265 °C over 45 min.

Shell Precursor Stock Solutions. *Synthesis of Single-Injection InZnP Complex Precursor.* The precursor was prepared by a modified version of the approach of Ramasamy et al.[23] Indium acetate (1 mmol), zinc acetate (0.5 mmol), and oleic acid (4 mmol) were mixed with 8 mL of ODE in a 100 mL Schlenk flask. The reaction flask was degassed at 110 °C under vacuum for 4 h. The flask was then switched to nitrogen flow and cooled to room temperature. Subsequently, a solution containing 0.66 mmol of $(TMS)_3P$ and 1 mL of TOP was quickly injected into the flask and stirred at room temperature for 60 min. Finally, the flask was transferred to the glovebox for further use.

Synthesis of Single-Injection Pure InP Complex Precursor. The synthesis was carried out in a similar manner to that of the InZnP complex precursor, except that the Zn precursor was not added in the reaction.

TOP-Se. A saturated TOP-Se solution was prepared by mixing and stirring 1.78 g of selenium powder in 10 mL of TOP inside the glovebox.

Zn-Stearate in ODE. Zn-stearate (2.5 g) was dispersed in 10 mL of ODE and vortexed for 5 min inside the glovebox.

Ga-Oleate Solution. In a nitrogen-filled glovebox, $GaCl_3$ (0.3 mmol, 52.8 mg), oleic acid (1.2 mmol, 0.34 g), and 2 mL of ODE were magnetically stirred in a 5 mL vial at 100 °C for 30 min.

Absorption Measurements. The optical absorption measurements were performed with a PerkinElmer Lambda 950 UV−vis−NIR spectrophotometer. The solutions were placed in a quartz cuvette with a 1 mm path length. The absorption measurements were done by evaporating the initial *n*-octane under a constant flow of nitrogen using a nitrogen gun and then redispersing the dots in C_2Cl_4 prior to measurement.

Photoluminescence Quantum Yield (PLQY) and Time-Resolved PL Measurements. The steady state photoluminescence measurements were performed with a Horiba Fluorolog Time Correlated Single Photon Counting System equipped with UV−vis−NIR photomultiplier detectors, dual grating spectrometers, and a monochromatized xenon lamp excitation source. The samples were

https://dx.doi.org/10.1021/acs.chemmater.9b05110
Chem. Mater. XXXX, XXX, XXX−XXX

excited at 700 nm using a 500 W xenon lamp. A published method[24] was used to measure quantum yields using an integrating sphere. Light was coupled into the Fluorolog system, and the integrating sphere was coupled with optical fiber bundles. Time-resolved PL measurements were performed by exciting the samples with a 723 nm laser.

Ultrafast Transient Absorption Spectroscopy. A Yb:KGW regenerative amplifier (Pharos, Light Conversion) produced the 1030 nm fundamental (5 kHz). A portion of the beam was passed through an optical parametric amplifier (Orpheus, Light Conversion) to generate the 800 nm pump pulse. Both the pump pulse and residual fundamental were sent into an optical bench (Helios, Ultrafast). The fundamental was sent through a delay stage, which determines the time delay between the two pulses, and then was focused into a sapphire crystal, generating a white light continuum. The pump pulse was sent through an optical chopper, reducing its frequency to 2.5 kHz. Both beams were then focused onto the sample. The probe light reflected off the mirror and was directed toward a CCD (Helios, Ultrafast).

X-ray Photoelectron Spectroscopy (XPS). XPS spectra were measured by using a Thermo Scientific K-Alpha System with an Al Kα source. The films were prepared on glass substrates. A 50 eV pass energy and scans were taken at 0.05 eV steps. The atomic ratios were obtained by integrating under the area of each peak and scaled by atomic sensitivity factors. We normalized all of the element areas with respect to Arsine (As) to obtain accurate atomic ratios.

TEM Measurements. All TEM images were acquired on a Hitachi HF 3300 electron microscope operating at 300 keV. TEM samples were prepared by drop casting a purified solution of QDs from *n*-octane onto a 300 mesh copper grid with a carbon film (SPI supplies). ImageJ was employed to generate the size of the dots.

XRD Measurement. XRD samples were prepared by drop casting a layer of the desired core or core/shell material from octane solution on a glass substrate. Measurements were performed on a Rigaku Powder Diffractometer.

RESULTS AND DISCUSSION

InAs QDs are prone to surface oxidation under ambient conditions, and this leads to a low PLQY (1−2%).[25,26] When InAs core QDs were stored under ambient conditions, we observed a gradual shift of the absorption spectra toward higher energies: the first excitonic peak, λ_{1S-1S}, moved from 1.32 to 1.38 eV over 3 weeks (see Supporting Information S1). This shift indicates the oxidation of As to As_2O_3, leading to a contraction of the InAs core size and an increase in the effective bandgap.[26] Similar oxidation processes are also observed in Pb-chalcogenide QDs such as PbSe and PbS.[27] These processes are a source of nonradiative recombination pathways leading to the loss of charge carriers and low efficiencies.

One strategy to improve the radiative recombination in QDs is the epitaxial growth of a wider-bandgap semiconductor on the surface of the QD.[16] Unfortunately, this often broadens the PL line widths, especially when shell thickness is increased. Additionally, interfacial defects form and the particle size distribution increases.[28] Even in the case of nearly lattice-matched InAs/CdSe QDs, PL line widths broaden as the CdSe shell thickness is increased.[29] If Zn-based shells are used, the larger lattice mismatch restricts the shell thickness to few monolayers.

To overcome the broad line widths and grow thicker shells, we developed an approach to grow multiple shells on InAs QDs: multishelling results in better confinement of the electron and hole while simultaneously distributing the lattice strain more evenly across the entire shell.[30] This enables the growth of thicker shells (Figure 1).

We began by growing a wider-bandgap InZnP shell: Zn incorporation into InP resulted in better surface passivation, a finding previously established in InP core−shell QDs[31] (see Supporting Information, Table S1, for lattice mismatch). We utilized a single-precursor complex of InZnP to grow InZnP shells (see Experimental Section for details). The rate of addition of the shell precursor resulted in a growth rate of a monolayer thickness per ∼10 min, similar to the rate used in the successive ionic layer absorption and reaction (SILAR) technique.[32] Additionally, use of a single precursor ensures a continuous supply of monomers.[33] This enabled the growth of a uniform shell that maintained the size dispersion of dots (σ = 6%). The temperature of shell growth was chosen to be 265 °C, as the starting InAs core QDs in the presence of oleylamine and octadecene showed good thermal stability at 270 °C: Ostwald ripening was not observed at this temperature (Supporting Information S2).[34] We note that high-quality InP QDs are synthesized around 270 °C.[17] These shell growth conditions ensured formation of a zinc blende crystalline InZnP shell.

We have introduced a wider-bandgap GaP shell, which enables better confinement of carriers. An additional GaP layer is commonly used for InP QDs to further enhance the PLQY,[18,19] but GaP shells have not been grown on InAs QDs. Finally, a ZnSe shell was added to prevent the oxidation of the GaP layer.

We show that the changes in absorption spectra are not due to Ostwald ripening of InAs QDs: when InAs QDs are heated at 270 °C in the presence of oleylamine and ODE without shell precursors, there is little shift in the absorption peak position (see Figure S2). This shell growth occurs for the various sizes of InAs core QDs: we also show the growth of InZnP/ZnSe shells on smaller InAs core QDs (see Figure S3).

Recent reports indicate that the addition of a GaP layer on InP QDs improved the PLQY due to better confinement of carriers.[18,19] We observed that, upon the addition of Ga^{3+} (during the GaP layer growth) to the InAs/InZnP QDs, there was a gradual shift of the absorption and PL spectra to higher energies.[18] The growth of more than two monolayers of GaP results in destabilization of the colloid, leading to precipitation of the dots. To ensure the stability of GaP against oxidation, we grew a final shell of ZnSe. Figure 2c,d shows the PL and absorption spectra of InAs core QDs before and after the shell growth. It is notable that the excellent size dispersion of the starting quantum dots is maintained even during shell growth. The PL line widths are invariant with shell growth, and the absorption spectra clearly retain the band edge transition. Taken together, the PL and absorption spectra confirm the multishell growth of InAs QDs.

Powder X-ray diffraction (XRD) studies of InAs core QDs and core/shell QDs at different stages of the shell growth are shown in Figure 3a. The peak positions of InAs core QDs agree well with bulk InAs, confirming the cubic zincblende crystal structure. After the InZnP shell growth, the peaks shift to higher 2θ values, corresponding to the bulk InP zincblende peaks.[35] Growth of the ZnSe shell results in a shift to larger diffraction angles, corresponding to their bulk counterpart.[15] The addition of shells result in a significant narrowing of (111) reflections, indicating that there is an increase in crystal domain size, which in turn suggests that shell growth happens in an epitaxial manner.

Figure 3b shows the evolution of the X-ray photoelectron spectroscopy (XPS) spectra of the As 3d peak of InAs core

https://dx.doi.org/10.1021/acs.chemmater.9b05110
Chem. Mater. XXXX, XXX, XXX−XXX

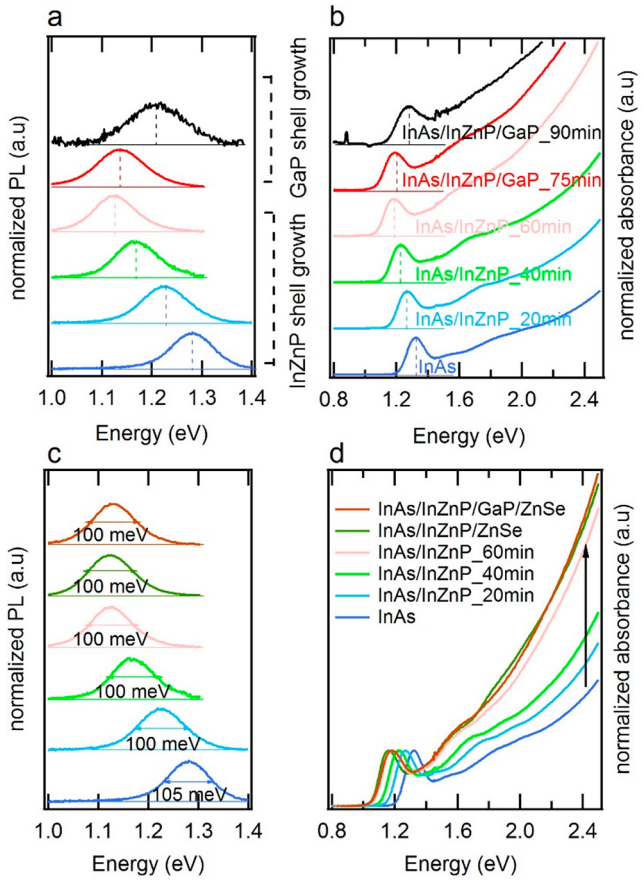

Figure 2. (a,b) Evolution of photoluminescence and absorption spectra of 3.1 nm InAs core QDs during the growth of InZnP and InZnP/GaP. Aliquots were taken at different time intervals to monitor the spectra. (c,d) Photoluminescence and absorption spectra of 3.1 nm InAs core QDs as well as InAs/InZnP/ZnSe and InAs/InZnP/GaP/ZnSe core/multishell QDs. All spectra have been normalized at the maximum of PL or absorption peak. Vertical offset is given for a clarity in graphs a–c.

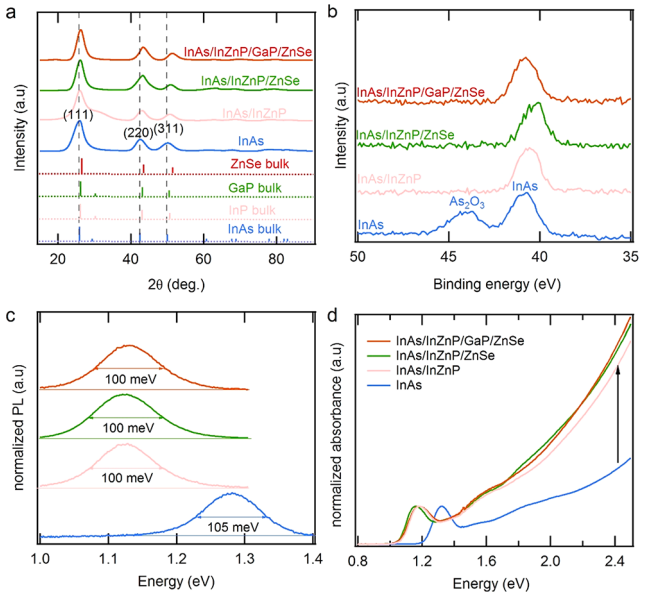

Figure 3. (a) X-ray diffractograms of InAs QDs before and during the growth stages of shell growth. The solid (blue) lines indicate the diffraction patterns of bulk semiconductors. The dashed lines (black) are added as a guide to show the shifts in 2θ values after the growth of different shells for the most intense reflections of (111), (220), and (311) planes of bulk InAs. (b) X-ray photoelectron spectroscopy (XPS) spectra of As 3d of InAs QDs before and after various stages of shell growth. (c,d) PL and absorption spectra of InAs QDs before and during the growth stages of shell growth.

QDs before and at various stages of shell growth on purified samples (see Experimental Section). The 3d peak of InAs core QDs shows two distinct peaks, which can be deconvolved into a lower energy peak at 40.8 eV corresponding to elemental As (63% contribution) and a higher energy peak at 44.4 eV corresponding to the oxidized species, As_2O_3 (37% contribution).[26] After the addition of the InZnP, there is an absence of As_2O_3 peaks, indicating a substantially complete shell that provides protection of the core from oxidation. In addition, we also analyzed the composition of 3.1 nm InAs core QDs and the resultant shelled QDs at every stage by XPS (see Supporting Information S4). Initial InAs core QDs are cation-rich with an In/As ratio of 1.4:1.[36] The growth of an InZnP shell showed the presence of a Zn 2p and P 2p peak as well as a strengthened In 3d peak. Addition of the GaP shell resulted in a decrease in the Zn 2p peak along with an increase in the P 2p peak and the appearance of Ga 3d signal. Figures S5 and S6 show the bright field TEM images of InAs/InZnP and InAs/InZnP/GaP QDs, respectively. The morphology and size of the dots remain the same before and after the growth of the GaP shell with an estimated diameter of 4.2 nm (σ = 7%). Several mechanisms have been proposed for the addition of GaP in the case of InP/GaP QDs.[18,19,37] Elemental composition and structural analysis suggest that GaP growth happens via a cation exchange method. The growth of an outer ZnSe shell results in an increase of the overall Zn 2p peak and the appearance of the Se 3d peak. We note that when a pure InP shell without Zn (see Supporting Information S7) is grown on InAs, we observed the peak attributed to As_2O_3. In addition, we invariably observe low PLQY in samples with a pure InP shell.[25] Taken together, these results indicate that a pure InP shell does not sufficiently passivate the InAs QDs. Figure 3c,d shows the PL and absorption spectra before and during the various stages of shell growth on InAs core QDs. Notably, our shell growth approach yields PL line widths ≈ 100 meV along with sharp absorption features.

Figure 4a–f shows the bright field, high-resolution TEM images and size histograms of InAs core QDs before and after the growth of InZnP/ZnSe and InZnP/GaP/ZnSe shells. The addition of shells results in an increase in the size of the QDs. As shown in Figure 4a,b, InAs core QDs have a quasispherical morphology with a diameter of 3.1 nm (σ = 8%), which correlates well with the sizing curve from literature. At higher magnifications (Figure 4b), lattice fringes can be seen. After the growth of multishells, there is an increase in the size of InAs/InZnP/ZnSe and InAs/InZnP/GaP/ZnSe QDs with estimated diameters of 5.5 (σ = 6%) and 6.0 nm (σ = 6%), respectively (see Figure 4c–f). The morphology of the dots is retained after the shell growth, and HR-TEM images exhibit well-resolved lattice fringes under different orientations Additionally, these images also confirm that shell growth is epitaxial, resulting in a single coherent lattice. Figure 4g,h shows a representative scanning transmission electron microscope (STEM) image of InAs/InZnP/GaP/ZnSe QDs under different magnifications.

To assess the efficacy of different shell growth approaches, we utilized transient PL and transient absorption spectroscopy

https://dx.doi.org/10.1021/acs.chemmater.9b05110
Chem. Mater. XXXX, XXX, XXX–XXX

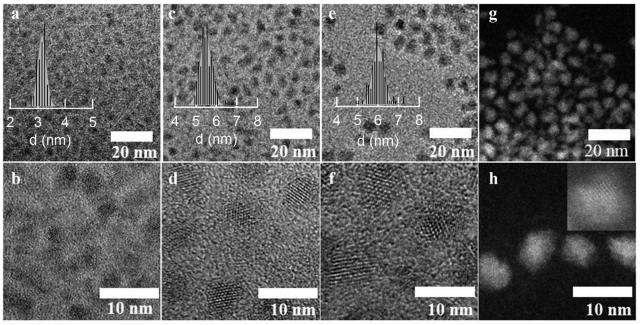

Figure 4. (a,c,e) Bright field TEM images along with the size histogram of the 3.1 nm InAs core, InAs/InZnP/ZnSe, and InAs/InZnP/GaP/ZnSe QDs, respectively. (b,d,f) HR-TEM images of the same showing lattice fringes. (g,h) STEM image of InAs/InZnP/GaP/ZnSe QDs under different magnifications. (Inset) High-resolution STEM image.

(TAS) measurements. PL decay traces (Figure 5a), fitted with a monoexponential fit, show increased lifetimes (τ) from 1.1 ns

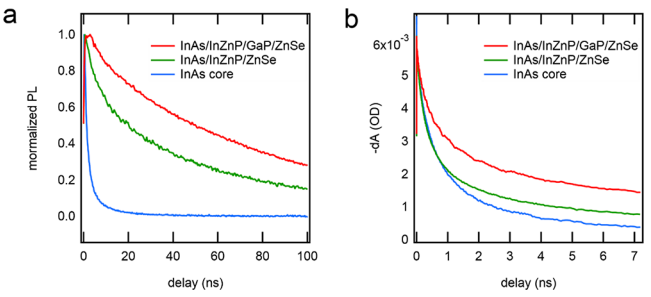

Figure 5. (a) Photoluminescence decay of InAs core, InAs/InZnP/ZnSe, and InAs/InZnP/GaP/ZnSe QDs, showing decreased nonradiative recombination rates in InAs/InZnP/GaP/ZnSe QDs, relative to InAs/InZnP/ZnSe QDs. (b) Normalized ground state bleach ($-dA$) kinetic traces with an average exciton occupancy of ~0.1, showing the slower population loss in the case of InAs/InZnP/GaP/ZnSe QDs.

for InAs core QDs to 10.2 and 12.4 ns upon the growth of InZnP/ZnSe and InZnP/GaP/ZnSe shells.[30] InAs core QDs are poor emitters with a low PLQY (~0.5%). As shown in Table 1, upon the growth of InZnP/ZnSe, the PLQY is

Table 1. Summary of PL Decay Lifetimes Showing Decreased Nonradiative Recombination Rates When a GaP Layer Is Added to InAs/InZnP/ZnSe QDs

parameter	InAs core	InAs/InZnP/ZnSe	InAs/InZnP/GaP/ZnSe
PLQY/%	0.5	14	23
τ/ns	1.1	10	12
$\Gamma_r/\mu s^{-1}$	4.8	13	18
$\Gamma_{nr}/\mu s^{-1}$	950	84	62

increased to 14%. The addition of the GaP layer in the case of InZnP/GaP/ZnSe further improves the PLQY to 23%. Introducing a thin GaP layer has been shown to improve the PLQY of InP/ZnS QDs;[18,19] similarly, our results indicate that GaP improves the surface passivation of InAs core QDs. To eliminate the size effect, we have additionally synthesized InAs/InZnP/ZnSe QDs with an estimated diameter of 6.0 nm (Figure S8). We observed that 6.0 nm sized InAs/InZnP/ZnSe showed a similar PLQY of 14% to that of the 5.5 nm size InAs/InZnP/ZnSe QDs. Based on these findings, we conclude that the improved PL in the case of InAs/InZnP/GaP/ZnSe QDs is attributed to the presence of GaP. The radiative recombination rate constant (Γ_r) of 3.1 nm InAs core QDs is 4.8 μs^{-1}; upon shelling with InZnP/ZnSe and InZnP/GaP/ZnSe, the rate increases to 13.2 and 18.1 μs^{-1}, respectively. Simultaneously, the nonradiative recombination rate constant (Γ_{nr}) decreases from 950 μs^{-1} (InAs core QDs) to 84 and 62 μs^{-1}, respectively. Normalized ground state bleach signals at sufficiently low fluences where $\langle N \rangle \approx 0.1$ are presented in Figure 5b, showing a longer carrier lifetime with the addition of a GaP layer. The bleach kinetic traces were fit using a biexponential model, and the parameters are given in Table S2. The bleach decay is due to direct surface trapping, and the decrease of the fractional contribution from this channel shows the benefit of adding a GaP layer. TAS data at higher fluences are also presented in Figure S9. It was previously shown for InAs/ZnSe core/shell QDs that these transients are associated with the rapid transfer of electrons from the conduction band to surface trap states.[38] PLQY, PL decay, and TAS measurements confirm that the addition of a GaP shell provides improved surface passivation and decreases the nonradiative recombination pathways.

CONCLUSIONS

This work reports the synthesis of InAs/InZnP/ZnSe and InAs/InZnP/GaP/ZnSe QDs with narrow PL line widths of ~100 meV with an emission peak centered at 1.12 eV. Due to the use of a single-injection precursor method to grow intermediate InZnP shells, the multishell approach retains the narrow PL line widths and excellent surface passivation. The multishell approach, enabled only by the growth of an additional GaP layer, allowed us to improve the PLQY up to 23% while maintaining the excellent size distribution of the starting dots. This work represents the narrowest line width obtained from InAs QDs at this wavelength.

ASSOCIATED CONTENT

Supporting Information

The Supporting Information is available free of charge at https://pubs.acs.org/doi/10.1021/acs.chemmater.9b05110.

Information on the oxidation of the InAs core QDs with time; stability of InAs core QDs in the presence of oleylamine + ODE without any shell precursors at 270 °C; shell growth on small InAs core QDs with an absorption max of 1.63 eV; XPS results of InAs core, InAs/InZnP, InAs/InZnP/GaP, InAs/InZnP/ZnSe, and InAs/InZnP/GaP/ZnSe; TEM images of InAs/InZnP and InAs/InZnP/GaP QDs; InAs/InP/ZnSe QDs (without Zn during the InP shell growth); TEM images of 6 nm InAs/InZnP/ZnSe; PL decay traces (PDF)

AUTHOR INFORMATION

Corresponding Author

Edward H. Sargent − *Department of Electrical and Computer Engineering, University of Toronto, Toronto, Ontario M5S 3G4, Canada;* orcid.org/0000-0003-0396-6495; Email: ted.sargent@utoronto.ca

https://dx.doi.org/10.1021/acs.chemmater.9b05110
Chem. Mater. XXXX, XXX, XXX−XXX

Authors

Laxmi Kishore Sagar − *Department of Electrical and Computer Engineering, University of Toronto, Toronto, Ontario M5S 3G4, Canada;* orcid.org/0000-0002-7656-7308

Golam Bappi − *Department of Electrical and Computer Engineering, University of Toronto, Toronto, Ontario M5S 3G4, Canada*

Andrew Johnston − *Department of Electrical and Computer Engineering, University of Toronto, Toronto, Ontario M5S 3G4, Canada;* orcid.org/0000-0002-4545-532X

Bin Chen − *Department of Electrical and Computer Engineering, University of Toronto, Toronto, Ontario M5S 3G4, Canada*

Petar Todorović − *Department of Electrical and Computer Engineering, University of Toronto, Toronto, Ontario M5S 3G4, Canada;* orcid.org/0000-0002-2838-876X

Larissa Levina − *Department of Electrical and Computer Engineering, University of Toronto, Toronto, Ontario M5S 3G4, Canada*

Makhsud I. Saidaminov − *Department of Electrical and Computer Engineering, University of Toronto, Toronto, Ontario M5S 3G4, Canada;* orcid.org/0000-0002-3850-666X

F. Pelayo García de Arquer − *Department of Electrical and Computer Engineering, University of Toronto, Toronto, Ontario M5S 3G4, Canada*

Sjoerd Hoogland − *Department of Electrical and Computer Engineering, University of Toronto, Toronto, Ontario M5S 3G4, Canada*

Complete contact information is available at: https://pubs.acs.org/10.1021/acs.chemmater.9b05110

Notes

The authors declare no competing financial interest.

■ ACKNOWLEDGMENTS

This research was supported by the Ontario Research Fund-Research Excellence Program and by the Natural Sciences and Engineering Research Council (NSERC) of Canada.

■ REFERENCES

(1) Reed, M.; Randall, J.; Aggarwal, R.; Matyi, R.; Moore, T.; Wetsel, A. Observation of Discrete Electronic States in a Zero-Dimensional Semiconductor Nanostructure. *Phys. Rev. Lett.* **1988**, *60* (6), 535−537.

(2) Kippeny, T.; Swafford, L. A.; Rosenthal, S. J. Semiconductor Nanocrystals: A Powerful Visual Aid for Introducing the Particle in a Box. *J. Chem. Educ.* **2002**, *79* (9), 1094−1100.

(3) Grim, J. Q.; Manna, L.; Moreels, I. A Sustainable Future for Photonic Colloidal Nanocrystals. *Chem. Soc. Rev.* **2015**, *44* (16), 5897−5914.

(4) Kagan, C. R.; Lifshitz, E.; Sargent, E. H.; Talapin, D. V. Building Devices from Colloidal Quantum Dots. *Science* **2016**, *353* (6302), No. aac5523.

(5) Yang, Z.; Voznyy, O.; Liu, M.; Yuan, M.; Ip, A. H.; Ahmed, O. S.; Levina, L.; Kinge, S.; Hoogland, S.; Sargent, E. H. All-Quantum-Dot Infrared Light-Emitting Diodes. *ACS Nano* **2015**, *9* (12), 12327−12333.

(6) Klimov, V. I.; Mikhailovsky, a a; Xu, S.; Malko, A.; Hollingsworth, J. a; Leatherdale, C. a; Eisler, H.; Bawendi, M. G. Optical Gain and Stimulated Emission in Nanocrystal Quantum Dots. *Science* **2000**, *290* (5490), 314−317.

(7) Hoogland, S.; Sukhovatkin, V.; Howard, I.; Cauchi, S.; Levina, L.; Sargent, E. H. A Solution-Processed 1.53 Mum Quantum Dot Laser with Temperature-Invariant Emission Wavelength. *Opt. Express* **2006**, *14* (8), 3273−3281.

(8) Saran, R.; Curry, R. J. Lead Sulphide Nanocrystal Photodetector Technologies. *Nat. Photonics* **2016**, *10* (2), 81−92.

(9) Norton, P. Third-Generation Sensors for Night Vision. *Optoelectron. Rev.* **2006**, *14* (1), 1−10.

(10) Rogach, A. L.; Eychmüller, A.; Hickey, S. G.; Kershaw, S. V. Infrared-Emitting Colloidal Nanocrystals: Synthesis, Assembly, Spectroscopy, and Applications. *Small* **2007**, *3* (4), 536−557.

(11) Carey, G. H.; Abdelhady, A. L.; Ning, Z.; Thon, S. M.; Bakr, O. M.; Sargent, E. H. Colloidal Quantum Dot Solar Cells. *Chem. Rev.* **2015**, *115* (23), 12732−12763.

(12) Li, J.; Zhu, J.-J. Quantum Dots for Fluorescent Biosensing and Bio-Imaging Applications. *Analyst* **2013**, *138* (9), 2506.

(13) Reiss, P.; Carrière, M.; Lincheneau, C.; Vaure, L.; Tamang, S. Synthesis of Semiconductor Nanocrystals, Focusing on Nontoxic and Earth-Abundant Materials. *Chem. Rev.* **2016**, *116* (10), 10731−10819.

(14) Xu, G.; Zeng, S.; Zhang, B.; Swihart, M. T.; Yong, K.-T.; Prasad, P. N. New Generation Cadmium-Free Quantum Dots for Biophotonics and Nanomedicine. *Chem. Rev.* **2016**, *116* (19), 12234−12327.

(15) Srivastava, V.; Kamysbayev, V.; Hong, L.; Dunietz, E.; Klie, R. F.; Talapin, D. V. Colloidal Chemistry in Molten Salts: Synthesis of Luminescent In1-XGaxP and In1- XGaxAs Quantum Dots. *J. Am. Chem. Soc.* **2018**, *140* (38), 12144−12151.

(16) Reiss, P.; Protière, M.; Li, L. Core/Shell Semiconductor Nanocrystals. *Small* **2009**, *5* (2), 154−168.

(17) Li, Y.; Hou, X.; Dai, X.; Yao, Z.; Lv, L.; Jin, Y.; Peng, X. Stoichiometry-Controlled InP-Based Quantum Dots: Synthesis, Photoluminescence, and Electroluminescence. *J. Am. Chem. Soc.* **2019**, *141* (16), 6448−6452.

(18) Pietra, F.; Kirkwood, N.; De Trizio, L.; Hoekstra, A. W.; Kleibergen, L.; Renaud, N.; Koole, R.; Baesjou, P.; Manna, L.; Houtepen, A. J. Ga for Zn Cation Exchange Allows for Highly Luminescent and Photostable InZnP-Based Quantum Dots. *Chem. Mater.* **2017**, *29* (12), 5192−5199.

(19) Kim, S.; Kim, T.; Kang, M.; Kwak, S. K.; Yoo, T. W.; Park, L. S.; Yang, I.; Hwang, S.; Lee, J. E.; Kim, S. K.; et al. Highly Luminescent InP/GaP/ZnS Nanocrystals and Their Application to White Light-Emitting Diodes. *J. Am. Chem. Soc.* **2012**, *134* (8), 3804−3809.

(20) Cao, Y. W.; Banin, U. Growth and Properties of Semiconductor Core/Shell Nanocrystals with InAs Cores. *J. Am. Chem. Soc.* **2000**, *122* (40), 9692−9702.

(21) Aharoni, A.; Mokari, T.; Popov, I.; Banin, U. Synthesis of InAs/CdSe/ZnSe Core/Shell1/Shell2 Structures with Bright and Stable Near-Infrared Fluorescence. *J. Am. Chem. Soc.* **2006**, *128* (1), 257−264.

(22) TaMang, S.; Lee, S.; Choi, H.; Jeong, S. Tuning Size and Size Distribution of Colloidal InAs Nanocrystals via Continuous Supply of Prenucleation Clusters on Nanocrystal Seeds. *Chem. Mater.* **2016**, *28* (22), 8119−8122.

(23) Ramasamy, P.; Ko, K. J.; Kang, J. W.; Lee, J. S. Two-Step "Seed-Mediated" Synthetic Approach to Colloidal Indium Phosphide Quantum Dots with High-Purity Photo- and Electroluminescence. *Chem. Mater.* **2018**, *30* (11), 3643−3647.

(24) de Mello, J. C.; Wittmann, H. F.; Friend, R. H. An Improved Experimental Determination of External Photoluminescence Quantum Efficiency. *Adv. Mater.* **1997**, *9* (3), 230−232.

(25) Xie, R.; Chen, K.; Chen, X.; Peng, X. InAs /InP /ZnSe Core/Shell /Shell Quantum Dots as Near-Infrared Emitters: Bright, Narrow-Band, Non-Cadmium Containing, and Biocompatible. *Nano Res.* **2008**, *1* (6), 457−464.

(26) Song, J. H.; Choi, H.; Pham, H. T.; Jeong, S. Energy Level Tuned Indium Arsenide Colloidal Quantum Dot Films For Efficient Photovoltaics. *Nat. Commun.* **2018**, *9* (1), 4267.

(27) Beygi, H.; Sajjadi, S. A.; Babakhani, A.; Young, J. F.; van Veggel, F. C. J. M. Surface Chemistry of As-Synthesized and Air-Oxidized PbS Quantum Dots. *Appl. Surf. Sci.* **2018**, *457*, 1−10.

(28) Hollingsworth, J. A.; Klimov, V. I. "Soft" Chemical Synthesis and Manipulation of Semiconductor Nanocrystals. *Nanocrystal Quantum Dots* **2010**, 1−61.
(29) Bertram, S. N.; Spokoyny, B.; Franke, D.; Caram, J. R.; Yoo, J. J.; Murphy, R. P.; Grein, M. E.; Bawendi, M. G. Single Nanocrystal Spectroscopy of Shortwave Infrared Emitters. *ACS Nano* **2018**, *13* (2), 1042−1049.
(30) Wijaya, H.; Darwan, D.; Lim, K. R. G.; Wang, T.; Khoo, K. H.; Tan, Z. K. Large-Stokes-Shifted Infrared-Emitting InAs-In(Zn)P-ZnSe-ZnS Giant-Shell Quantum Dots by One-Pot Continuous-Injection Synthesis. *Chem. Mater.* **2019**, *31* (6), 2019−2026.
(31) Pietra, F.; De Trizio, L.; Hoekstra, A. W.; Renaud, N.; Prato, M.; Grozema, F. C.; Baesjou, P. J.; Koole, R.; Manna, L.; Houtepen, A. J. Tuning the Lattice Parameter of InxZny P for Highly Luminescent Lattice-Matched Core/Shell Quantum Dots. *ACS Nano* **2016**, *10* (4), 4754−4762.
(32) Li, J. J.; Wang, Y. A.; Guo, W.; Keay, J. C.; Mishima, T. D.; Johnson, M. B.; Peng, X. Large-Scale Synthesis of Nearly Monodisperse CdSe/CdS Core/Shell Nanocrystals Using Air-Stable Reagents via Successive Ion Layer Adsorption and Reaction. *J. Am. Chem. Soc.* **2003**, *125* (41), 12567−12575.
(33) Friedfeld, M. R.; Johnson, D. A.; Cossairt, B. M. Conversion of InP Clusters to Quantum Dots. *Inorg. Chem.* **2019**, *58* (1), 803−810.
(34) Franke, D.; Harris, D. K.; Chen, O.; Bruns, O. T.; Carr, J. A.; Wilson, M. W. B.; Bawendi, M. G. Continuous Injection Synthesis of Indium Arsenide Quantum Dots Emissive in the Short-Wavelength Infrared. *Nat. Commun.* **2016**, *7*, 12749.
(35) Cao, Y.; Banin, U. Synthesis and Characterization of InAs/InP and InAs/CdSe Core/Shell Nanocrystals. *Angew. Chem., Int. Ed.* **1999**, *38* (24), 3692−3694.
(36) Srivastava, V.; Dunietz, E.; Kamysbayev, V.; Anderson, J. S.; Talapin, D. V. Monodisperse InAs Quantum Dots from Aminoarsine Precursors: Understanding the Role of Reducing Agent. *Chem. Mater.* **2018**, *30* (11), 3623−3627.
(37) Wegner, K. D.; Pouget, S.; Ling, W. L.; Carrière, M.; Reiss, P. Gallium - A Versatile Element For Tuning The Photoluminescence Properties of InP Quantum Dots. *Chem. Commun.* **2019**, *55* (11), 1663−1666.
(38) Cadirci, M.; Stubbs, S. K.; Hardman, S. J. O.; Masala, O.; Allan, G.; Delerue, C.; Pickett, N.; Binks, D. J. Ultrafast Exciton Dynamics in InAs/ZnSe Nanocrystal Quantum Dots. *Phys. Chem. Chem. Phys.* **2012**, *14* (43), 15166−15172.

https://dx.doi.org/10.1021/acs.chemmater.9b05110
Chem. Mater. XXXX, XXX, XXX−XXX